Ab initio modeling of primary processes in photosynthesis : protein induced activation of bacteriochlorophylls for efficient light harvesting and charge separation

Wawrzyniak, P.K.

Chapter 4

Electronic Structure of Histidines in Bacterial Reaction Center

4.1 Introduction

This chapter presents an assignment of protonation states and interpretation of NMR spectra for histidines in *Rhodobacter sphaeroides* bacterial reaction centers. As discussed in the general introduction, the asymmetry of the special pair both in the ground state and in the excited state may facilitate the asymmetric electron transfer along the cofactor branches. Although a number of studies on the role of the protein environment in the electron transfer do exist [104, 105], a precise indication of the effects induced by the neighboring residues is still missing. [106, 107] Solid-state NMR combined with quantum chemical calculations is a powerful technique able to resolve electronic structure of residues, even in large membrane proteins like for instance the LH2 complex. [26, 39, 108] Here an interpretation of SSNMR spectra for the four Mg-coordinated and twelve other histidines in the BRC is proposed, based on the theoretical prediction of chemical shifts. It is established that all the axial BChl *a*-ligating histidines exist in the neutral$_\pi$ form. Interestingly, one of

them has a special electronic structure, different from the other three, which is attributed to the presence of a hydrogen-bonded water at the N_π nitrogen, effectively breaking the overall symmetry of those four histidines. [50] According to the calculations such interaction causes a reorganization of electronic density within the imidazole ring, affecting all the atoms. That, in turn, brings the coordinated histidine and bacteriochlorophyll *a* closer together. This structure modification may have a significant effect on the electron transfer properties. Also chemical shifts of non-axial histidines are investigated. It is proposed that in addition to several neutral$_\tau$ histidines, two groups of cationic histidines exist: doubly protonated and doubly protonated with hydrogen bonds at N_π and N_τ. The last group is characterized by a downfield shifted C_δ resonance.

4.2 Models and Methods

The Density Functional Theory calculations were performed using the Gaussian 03 package [80] and the BLYP [73,75,76] exchange-correlation functional in combination with the 6-311++G(d,p) basis set. This approach has been found to be an optimal trade-off between computational cost and accuracy in order to be accurate enough to confirm and validate experimental findings for light-harvesting complex II. [108] It was established that DFT calculations can predict accurately chemical shift differences between different histidine protonation states, although the deviation from the experiment in the absolute values may be large, especially for ^{15}N chemical shifts. Histidine in various protonation states of the imidazole ring were considered and their geometry was fully optimized, yielding cationic and neutral$_\pi$ histidine with an internal hydrogen bond between N_π and the carbonyl group of the tail.

To model the axial histidines the BChl *a*–His complex was extracted from the 1M3X crystal structure of the *Rhodobacter sphaeroides* reaction center. [50] The model incorporates P_L, His L173 and the water 1007 molecule to study the effect of the hydrogen bond at the N_π nitrogen of histidine. To model histidines in a protein environment, a neutral amino acid termination (COOH–NH_2) was used to saturate the broken peptide bond. The phytyl tail of the bacteriochlorophyll *a* was truncated at the esther group and saturated

by a hydrogen atom in the model. Neither the electronic structure of histidine side chain, nor the electronic structure of the porphyrin ring is affected by these truncations.

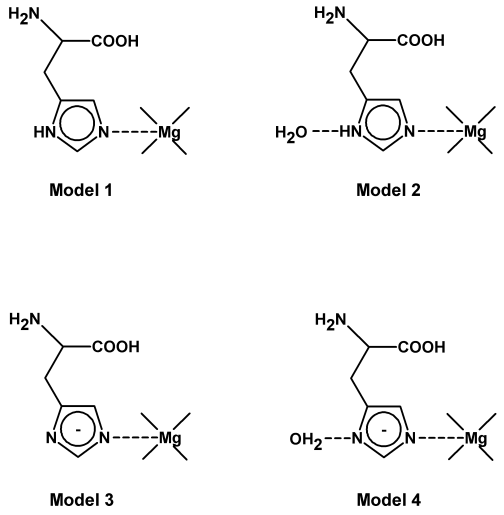

Figure 4.1: The models of BChl *a*–His complexes in various protonation states. In the schematic representation of the model, the remaining part of the BChl *a* molecule was omitted for clarity. The indicated charge of histidine is the formal charge.

Four models were considered, as shown in Fig 4.1, accounting for possible protonation states of the histidine side-chain and presence or absence of the hydrogen bond: Model **1** including BChl *a* and His in the neutral$_\pi$ form; Model **2** obtained by adding to model **1** the water molecule hydrogen bonded to His L173; Model **3** and **4** similarly to model **1** and **2**, respectively, but with the histidine ring deprotonated (formally anionic). The geometries of all the models were partially optimized by relaxing the atomic positions of the imidazole ring, the Mg atom and the two hydrogens of the water molecule, while keeping all the other atomic coordinates fixed to the crystallographic data. These constraints were introduced in order to maintain the geometric shape of the complex induced by the protein environment.

Chemical shifts were calculated using the GIAO method for all the models. [82–85] The ^{1}H and ^{13}C chemical shifts were referred to TMS, while the

^{15}N chemical shifts were referred to $^{15}NH_3$ and are all reported in ppm. The ADF program [87–89] was used to calculate the electron density difference map between the BChl *a*-His-H2O complex (**2**) and the two fragments: BChl *a*-His and water, in order to characterize the electron density perturbation induced by the presence of the hydrogen bond. The BLYP functional with the TZP basis set was used for this calculation.

4.3 Results and Discussion

The recorded 2D ^{1}H-^{13}C dipolar correlation spectrum of [^{13}C,^{15}N]-histidine labeled reaction centers is presented in Figure 4.2 and the experimental chemical shifts are collected in Table 4.1, together with theoretically predicted chemical shifts for various BChl *a*–His complexes. The four BChl *a*-coordinated histidines are clearly separated from the non-axial ones by the upfield shift of H_δ and H_ε signals due to ring current effects experienced by the atoms close to the conjugated porphyrin system of BChl *a*. The non-axial residues

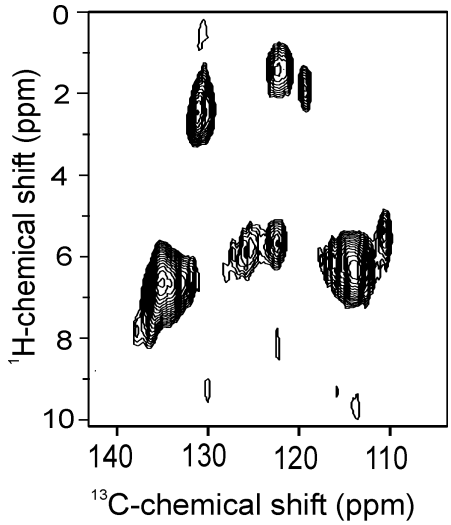

Figure 4.2: Contour plot sections of 2D heteronuclear ^{1}H-^{13}C dipolar correlation spectrum of [^{13}C,^{15}N]-histidine labeled bacterial reaction centers collected in a magnetic field strength of 17.6 T. Courtesy of A. Alia

resonate in the range of ≃5–8 ppm, while the signals from the axial histidines

	Experiment			DFT				
	Type 1	Type 2	$\Delta\delta_{type1-type2}$	**1** 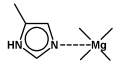	**2** 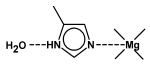	$\Delta\delta_{1-2}$	**3** 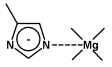	**4** 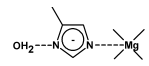
C_γ				131.6	131.7	−0.1	139.5	138.2
C_δ	121.9	119.1	2.8	128.6	127.6	1.0	120.1	120.4
C_ε	130.9	129.9	1.0	135.8	136.0	−0.2	145.3	144.3
C_ε -C_δ	9.0	10.8	−1.8	7.2	8.4	−1.2	25.2	23.9
N_π				189	200	−11	303	284
N_τ	225	220	5	268	265	3	244	246
H_δ	1.5	1.9	−0.4	4.0	4.0	0.0	3.8	3.7
H_ε	2.5	2.4	0.1	3.4	3.2	0.2	3.4	3.3

Table 4.1: Comparison between experimental chemical shifts [ppm] of axial histidines in BRC with theoretically predicted values for the different BChl *a*–His complexes considered in this work. The difference between models **1** and **2** ($\Delta\delta_{1-2}$) and the difference between the experimental data for Type 1 and Type 2 histidines ($\Delta\delta_{type1-type2}$) are also reported. In the schematic representation of the model, the histidine tail and the remaining part of the BChl *a* molecule were omitted for clarity. The indicated charge of histidine is the formal charge.

appear between ≃1–3 ppm. This ring current shift is reproduced by the calculations, as may be noticed by comparing the ^{1}H chemical shifts for BChl *a*–His complex in Table 4.1 with the chemical shifts for uncoordinated histidines in Table 3.1. The signals around 120 ppm are assigned to C_{δ}, while those around 130 ppm to C_{ε}.

4.3.1 Axial histidines

The upper part of the 2D NMR correlation spectrum, which concerns the signals from the axial histidines, will be considered first. From the analysis of the experimental and DFT-computed C_{ε} - C_{δ} chemical shift differences presented in Table 4.1 it is immediately visible that the N_{π} atom is protonated in all the axial histidines. The presence of negatively charged histidine would produce C_{δ} and C_{ε} NMR signals separated by $\sim$ 25 ppm (models **3** and **4**), while in the BRC those signals are experimentally observed only $\sim$ 10 ppm apart, in good agreement with the prediction for the BChl *a*–His complex with formally neutral$_{\pi}$ histidine (models **1** and **2**). Therefore it may be concluded that the axial histidines in BRC are formally neutral$_{\pi}$. This conclusion is particularly relevant since it has been recently suggested that anionic histidines may be present in Photosystem II, where they may play an important functional role. [79] In spite of similarities between the two systems, in BRC there is no evidence of such unusual histidine charge state.

Interestingly, both C_{δ} and C_{ε} peaks appear clearly at two distinct positions in the ^{13}C dimension. In the ^{1}H dimension, the C_{δ} signals exhibit slightly different values as well. This suggests the existence of two types of axial histidines with slightly different electronic structure and they are labeled as Type 1 and Type 2, respectively, in the first two columns of Table 4.1. From the intensity integration it follows that the ratio between these two types is 3:1.

Figure 4.3 presents one-dimensional ^{15}N NMR spectrum of reaction centers with $^{15}N_{\tau}$– or uniformly ^{15}N– labeled histidines. The signals between 170 and 180 ppm are assigned to pyrrole-type nitrogens with or without a hydrogen bond, respectively; signals between 250 and 260 ppm are assigned to various pyridine-type nitrogens, and finally the signal at 225 ppm can be attributed to N_{τ} of the Mg-coordinated histidines. [26,39] Interestingly, an ad-

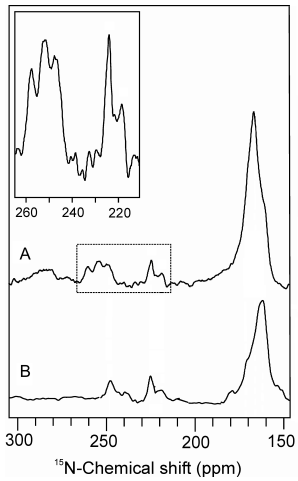

Figure 4.3: CP-MAS ^{15}N NMR spectra of uniformly ^{15}N– (A) and $^{15}N_{\tau}$– (B) histidine labeled reaction centers measured in a magnetic field of 17.6 T at 220 K. Detailed view of the region between 205 and 265 ppm is shown in the inset. Courtesy of A. Alia

ditional small peak from the Mg-coordinated N_{τ} atom is present at 220 ppm. Intensity fitting suggests, consistent with the ^{1}H-^{13}C correlation data, that there are two types of axial histidines: three resonate at 225 ppm, while the fourth one resonates with 220 ppm chemical shift. This indicates again the existence of one axial histidine with a special electronic structure different from the other three. A set of nucleus independent chemical shift (NICS) [109] calculations was performed to elucidate whether the ring current effect could be responsible for this difference. The used BChl *a* structure was the partially optimized DFT structure from model **2**, where the Mg–N_{τ} distance and Mg–N_{τ}–N1 angle are 2.184 Å and 97.70°, respectively. Additionally, several points in space with the Mg–N_{τ} distances ranging from 2.10 Å to 2.35 Å and Mg–N_{τ}–N1 angles between 90° and 105° were selected to sample various positions as the screening effect is expected to be highly anisotropic. These values correspond to typical values observed in X-ray data. [110] NICS calculations predict that the variation in the ring current shift between the different positions explored is within 0.4 ppm, therefore the observed 5 ppm upfield shift cannot be explained in terms of the ring current effect.

The DFT calculations for models **1** and **2** presented in Table 4.1 suggest

that the observed differences between Type 1 and Type 2 histidines can be explained by the presence of a strong hydrogen bond at the N_π nitrogen of the histidine. The formation of such a hydrogen bond results in polarization of the N_π–H bond towards the water molecule and higher electron density around the nitrogen. The 'excess' of electron density is then redistributed along the imidazole ring affecting all the atoms, as presented in Fig. 4.4. It can be especially seen that the ring bonds involving the N_π nitrogen are shorter. The N_τ signal is predicted to shift upfield by 3 ppm (experimentally

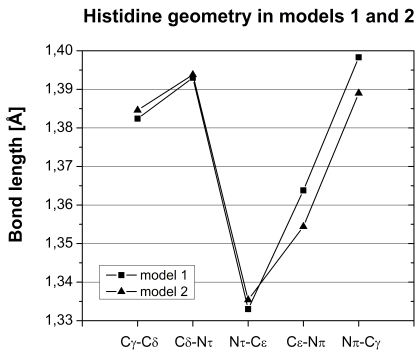

Figure 4.4: Selected bond lengths [Å] in the axial histidine models **1** and **2**.

5 ppm) and the C_δ and C_ε signal separation is slightly larger for the H-bound histidine (Table 4.1). The special histidine (Type 2) is also closer to the bacteriochlorophyll *a*, with the Mg–N_τ distance shorter by 0.034 Å compared to the other three histidines. Fig. 4.5 shows the change in the electronic density for complex **2** reflecting the polarization effects of the hydrogen-bonded water molecule. However, this does not take into account geometry changes upon hydrogen bond formation.

The results strongly suggest that the electronic structure of one of the axial histidines may be different due to the presence of a hydrogen bond at N_π. According to the crystal structure [50] two of the four axial histidines, His M202 and His L173, are within hydrogen-bonding distance to a water molecule with their N_π atoms, however, based on the data presented above

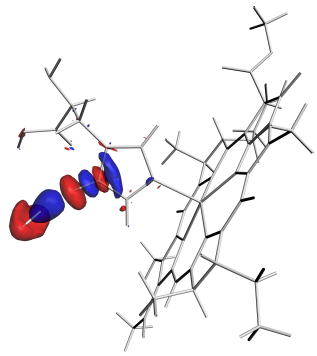

Figure 4.5: Change in electronic density reflecting the polarization effects of the hydrogen-bonding water molecule, calculated for model **2**. The isosurface value is 0.001 e/Å^3. Red corresponds to an increase of the density, as compared to the separated BChl *a*–His and water fragments, while blue denotes a decrease in the electronic density. Geometry changes upon hydrogen bond formation are not included.

it is not possible to say with certainty which of the two is the significantly different one.

4.3.2 Non-axial histidines

Apart from the four axial histidines, there are also 16 non-axial histidines present in the bacterial reaction center and 4 of them, namely His M219, His M266, His L190 and His L230, are located in the vicinity of Fe^{2+}. [50] Due to paramagnetic properties of iron, they are not visible on the spectrum in Figure 4.2. NMR signals of the remaining 12 histidines are present in the lower part of the spectrum. It is possible to partially assign the peaks using experimental data for crystalline histidines [26], however for a more complete assignment theoretical modeling is a crucial complementary tool. Therefore DFT calculations were performed for various protonation states of histidine imidazole ring and the results are presented in Table 4.2.

From the comparison with the experimental spectra it is evident that the presence of doubly deprotonated histidine can be ruled out because a very characteristic C_ε chemical shift, about 20 ppm downfield from the other forms, is not observed. Moreover, anionic histidine is energetically very unfavorable,

	C_δ	C_ε
cationic+2H_2O	124.9	130.9
cationic	122.6	132.9
neutral$_\tau$	117.9	136.0
neutral$_\pi$	134.5	137.3
anionic	133.4	154.0

Table 4.2: Calculated C_δ and C_ε chemical shifts for various protonation states of histidine.

which makes its existence highly improbable, unless some specific stabilization is provided by the protein environment, as proposed for Photosystem II. [79] The best correlation between experimental and calculated values (Fig. 4.7) shows that a large number of histidines occur in the neutral$_\tau$ form and give resonances at 113.6 (C_δ) and 134.9 (C_ε) ppm. A second group can be identified as doubly protonated histidines, which produce signals at 122.3 and 132.5 ppm for C_δ and C_ε, respectively. It is possible that some histidines are of the neutral$_\pi$ type which is predicted to resonate above 130 ppm with C_δ and C_ε signals separated by only $\sim$3 ppm. However, it is difficult to clearly distinguish them in the large group of signals visible on the spectrum in that range.

Interestingly, the calculations predict that if both N_τ and N_π nitrogens of cationic histidine are involved in hydrogen bonding, then a downfield shift of about 2.5 ppm is observed for C_δ. Thus, the peak at 125.7 ppm can be assigned to C_δ of this type of histidines with C_ε buried in the group of signals above 130 ppm. It is still a matter of debate whether the structural symmetry-breaking His L168, which is located in the close proximity of the active BChl *a*, could be attributed to the group of doubly hydrogen-bonded histidines. Mutation and FT Raman studies provided evidence that it is hydrogen bonded to Asn L166 on one side and to the 3^1 acetyl of P_L on the other side. [111,112] This, however, does not necessarily imply double protonation. To investigate this possibility, P_L, His L168 and Asn L166 were extracted from the 1M3X [50] crystal structure and two protonation models were tested. The first model contained His L168 in the neutral$_\tau$ form and the second one in the cationic form. Both of them were geometrically optimized, relaxing the histidine imidazole ring, asparagine amine and carbonyl groups, and the carbonyl group

of the bacteriochlorophyll *a* acetyl. The optimized model with His L168 in the neutral$_\tau$ form remains close to the geometry present in the crystal structure, while the orientation of Asn and His side chains changes considerably for doubly protonated His L168 (Fig. 4.6). Moreover, the X-ray data [50] displays

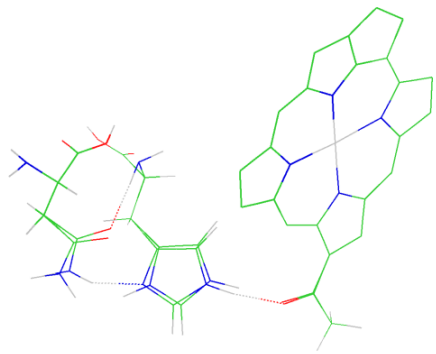

Figure 4.6: Comparison of partially optimized geometry for His L168 neutral and cationic. Relaxed atoms include histidine imidazole ring, asparagine amine and carbonyl groups and carbonyl group of the bacteriochlorophyll *a* acetyl. Representation of BChl *a* was simplified for clarity.

the asparagine amine group oriented towards the N_π nitrogen of the histidine, suggesting that His L168 is rather a hydrogen bond acceptor from the Asn L166 residue and a hydrogen bond donor to the P_L acetyl group. Therefore, this histidine can be classified to the group of neutral$_\tau$ histidines.

The shift of the remaining peak at 110.4 ppm is close to the calculated C_δ chemical shift of neutral$_\tau$ histidine, however the upfield shift cannot be explained by hydrogen bonds. Probably, a local electrostatic field of the protein is responsible for that unusual value. The overall correlation of the assignment is depicted in Figure 4.7 with a root mean square deviation of 3.6 ppm.

4.4 Conclusions

An assignment and interpretation of histidine NMR spectra in bacterial reaction centers was presented. It is established that all the axial histidines exist in the neutral$_\pi$ form and one of them has substantially different electronic

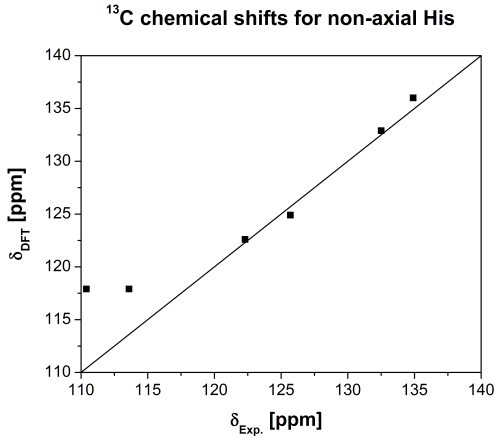

Figure 4.7: Correlation plot between calculated and experimental ^{13}C chemical shifts of non-axial histidines in bacterial reaction centers.

structure due to hydrogen-bonding with a water molecule at the N_π position. This effectively breaks the overall symmetry of those four histidines. From the presented data it is not possible to tell whether His L173 or His M202 is the distinct one but chapter **6** will revisit that problem providing further insight. The reorganization of the electronic density in the imidazole ring upon hydrogen bond formation affects all the ring atoms and is responsible for changes of their NMR chemical shifts. It is also predicted that such a special histidine is at closer distance to the Mg^{2+} than the other three. This special histidine may have a significant impact on the ground state asymmetry of the special pair, which can subsequently affect the excited state PES and thereby facilitate electron transfer and protein dynamics. This is important in view of recent progress revealing a strong role for the protein in the initial stages of the charge separation process. [113, 114] The DFT results are also used to propose an assignment of the non-axial histidines. In addition to the large number of neutral$_\tau$ histidines, two groups of cationic histidines are identified: doubly protonated and doubly protonated with hydrogen bonds at N_π and N_τ. It is not excluded that some neutral$_\pi$ histidines may be present as well. The structural symmetry-breaking histidine L168 is here identified as being of the neutral$_\tau$ type.